

**BUOYANT TURBULENT JETS AND PLUMES: III. ROUND TURBULENT  
NONBUOYANT STARTING JETS AND PUFFS  
AND BUOYANT STARTING PLUMES AND THERMALS**

R. Sangras and G. M. Faeth  
Department of Aerospace Engineering  
The University of Michigan  
Ann Arbor, Michigan 48109-2140

Prepared for:

U.S. Department of Commerce  
National Institute of Standards and Technology  
Laboratory for Building and Fire Research  
Washington, D.C. 20234

Annual Report  
Grant No. 60NANB8D0081  
H. R. Baum, NIST Scientific Officer

October 1999

### **Notice**

This report was prepared for the Laboratory for Building and Fire Research of the National Engineering Laboratory, National Institute of Standards and Technology, under Grant Number 60NANB80081. The statements and conclusions contained in this report are those of the authors and do not necessarily reflect the views of the National Institute of Standards and Technology, or the Laboratory for Building and Fire Research.

**BUOYANT TURBULENT JETS AND PLUMES: III. ROUND TURBULENT  
NONBUOYANT STARTING JETS AND PUFFS  
AND BUOYANT PLUMES AND THERMALS**

October 1999

Sponsored by:

U.S. Department of Commerce  
National Institute of Standards and Technology  
Laboratory for Building and Fire Research  
Washington, D.C. 20234

**BUOYANT TURBULENT JETS AND PLUMES:  
III. ROUND TURBULENT NONBUOYANT STARTING JETS AND PUFFS AND  
BUOYANT PLUMES AND THERMALS**

**Abstract**

A theoretical and experimental study of the temporal development of round turbulent nonbuoyant starting jets and puffs and buoyant starting plumes and thermals is described, limited to sources in still and unstratified environments. The experiments involved dye-containing salt or fresh water sources injected vertically downward into fresh water within a large windowed tank with injector passage length/diameter ratios of 50. Time-resolved video images of the flows were obtained using a CCD camera. Initial jet exit conditions were as follows: diameters of 3.2-12.7 mm, Reynolds numbers of 1450-11700 and jet/ambient density ratios of 1.00-1.12. Near-source behavior varied significantly with source properties but the flows generally became turbulent near the jet exit with self-preserving behavior generally observed at distances greater than 20-30 source diameters from the source. Within the self-preserving region, both the normalized streamwise penetration distance and the normalized maximum flow radius varied as function of time to the following powers:  $1/2$  (starting nonbuoyant jet),  $1/4$  (nonbuoyant puff),  $3/4$  (starting buoyant plume), and  $1/2$  (buoyant thermal).

## Acknowledgments

This research was supported by the U.S. Department of Commerce, National Institute of Standards and Technology, Grant No. 60NANB8D0081, with H. R. Baum of the Laboratory for Building and Fire Research serving as Scientific Officer.

## Table of Contents

	<u>Page</u>
Abstract .....	iv
Acknowledgments .....	v
List of Tables .....	vii
List of Figures.....	viii
Nomenclature.....	ix
1. Introduction.....	1
2. Experimental Methods .....	2
3. Theoretical Methods.....	4
4. Results and Discussion .....	8
5. Conclusions.....	20
References .....	24

## List of Tables

<u>Table</u>		<u>Page</u>
1	Summary of test conditions and scaling properties.....	4

## List of Figures

<u>Figure</u>	<u>Caption</u>	<u>Page</u>
1.	Sketch of round turbulent flows from steady and interrupted sources. ...	6
2.	Visualization of a round turbulent nonbuoyant starting jet ( $d=6.4$ mm, $u_o=46$ mm/s, $Re_o=2950$ ). .....	9
3.	Penetration distance as a function of time for round turbulent nonbuoyant starting jets. ....	11
4.	Flow radius as a function of penetration distance for round turbulent nonbuoyant starting jets. ....	12
5.	Visualization of a round turbulent nonbuoyant puff ( $d=6.4$ mm, $u_o=93$ mm/s, $Re_o=5900$ , $Q_o/(A_o d) = 50$ ). .....	13
6.	Penetration distance as a function of time for round turbulent nonbuoyant puffs. ....	15
7.	Flow radius as a function of penetration distance for round turbulent nonbuoyant puffs. ....	16
8.	Visualization of a round turbulent starting buoyant plume ( $d=6.4$ mm, $u_o=46$ mm/s, $Re_o=3200$ , $\rho_o/\rho_\infty = 1.076$ , $Fr_o = 7.0$ ). .....	17
9.	Penetration distance as a function of time for round turbulent buoyant starting plumes. ....	18
10.	Flow radius as a function of penetration distance for round turbulent buoyant starting plumes. ....	19
11.	Visualization of a round turbulent buoyant thermal ( $d=6.4$ mm, $u_o=46$ mm/s, $Re_o=3200$ , $\rho_o/\rho_\infty = 1.084$ , $Fr_o = 6.7$ , $Q_o/(A_o d) = 10$ ). .....	21
12.	Penetration distance as a function of time for round turbulent buoyant thermals. ....	22

13.	Flow radius as a function of penetration distance for round turbulent buoyant thermals. ....	23
-----	--	----

## Nomenclature

- $A_o$  = source cross sectional area
- $B_o$  = source buoyancy force, Eq. (10)
- $\dot{B}_o$  = source buoyancy flux, Eq. (9)
- $C_r$  = radial penetration coefficient, Eq. (4)
- $C_x$  = streamwise penetration coefficient, Eq (3)
- $d$  = source diameter
- $Fr_o$  = source Froude number, Eq. (2)
- $g$  = acceleration of gravity
- $l_M$  = Morton length scale, Eq. (1)
- $n$  = time exponent, Eq. (3)
- $Q_o$  = volume of injected source fluid
- $\dot{Q}_o$  = volumetric rate of injection of source fluid
- $Re_o$  = source Reynolds number,  $du_o/v_o$
- $r$  = radial distance
- $t$  = time
- $t^*$  = self-preserving time scales, Eqs. (5)-(8)
- $u$  = streamwise velocity
- $x$  = streamwise distance

$\nu$  = kinematic viscosity

$\rho$  = density

### **Subscripts**

max = maximum value

p = maximum penetration location

o = initial value or virtual origin

$\infty$  = ambient value

*l*

## 1. Introduction

A theoretical and experimental investigation of the temporal development of round turbulent nonbuoyant starting jets and puffs and buoyant starting plumes and thermals in still and unstratified environments is described. Study of these flows is motivated by practical applications to the unconfined and unsteady turbulent flows resulting from the initiation of steady and interrupted gas and liquid releases caused by process upsets, explosions and unwanted fires. Due to their simplicity, these flows also are of interest as classical fundamental configurations that illustrate the development of unsteady turbulent flows. As a result, observations of these flows are useful in order to provide data needed to evaluate methods of predicting their properties. Present experiments emphasized conditions far from the source where effects of source disturbances are lost, where flow structure is largely controlled by the conserved properties of the flow, and where the flow approximates self-preserving behavior. Particular advantages of self-preserving flow are that this region significantly simplifies both the presentation of experimental data and numerical simulations needed to evaluate models of the process.

Past experimental, theoretical and computational studies of round turbulent nonbuoyant starting jets and puffs and buoyant starting plumes and thermals have been reported by a number of workers, see Baines et al. (1990), Batt et al. (1984), Baum et al. (1994), Delichatsios (1979), Fay and Lewis (1976), Johari and Paduano (1987), Kato et al. (1987), Kouros et al. (1993), Kovaszny et al. (1974), List (1982), Morton et al. (1956), Pantzloff and Lueptow (1997), Richards (1965), Scorer (1957), Turner (1962, 1964, 1969, 1973) and references cited therein. These studies have provided self-preserving scaling rules that describe the main features of these flows but corresponding measurements of self-preserving flow properties are surprisingly limited. In addition, recent studies of the self-preserving properties of steady buoyant turbulent plumes due to Dai et al. (1994, 1995) and Sangras et al. (1998, 1999) show that self-preserving behavior generally is observed at distances farther from the source than previously thought (e.g., streamwise distances greater than roughly 100 source diameters). These observations raise additional concerns about existing measurements of the self-preserving behavior of round turbulent nonbuoyant and buoyant unsteady flows.

In view of the previous discussion, the present investigation considered the self-preserving properties of round turbulent nonbuoyant starting jets and puffs and buoyant starting plumes and thermals in still and unstratified environments. The specific objectives of the study were as follows:

- (i) Measure the streamwise and cross stream penetration properties of these flows as a function of time for various source diameters, source Reynolds numbers, source/ambient density ratios, source Froude numbers (for the buoyant flows), and amounts of injected source fluid (for the interrupted sources).
- (ii) Use the measured penetration properties to evaluate self-preserving scaling and to determine empirical factors needed to correlate penetration properties.

The experiments involved salt water sources having various salt concentrations injected into a still fresh water bath. Penetration properties were measured from flow visualizations consisting of time-resolved video records of dye-containing injected source liquids. Present observations extended to streamwise penetration distances on the order of 100 source diameters.

## 2. Experimental Methods

**Apparatus.** The experiments adopted methods of using salt water modeling of turbulent flows suggested by Steckler et al. (1986). The test apparatus consisted of a plexiglass (18 mm thick) tank open at the top. The water bath within the tank was rectangular and had inside plan dimensions of 610 x 724 mm and an inside depth of 432 mm. The bath was filled with fresh water to a depth of roughly 400 mm, using water from the laboratory water supply. The bath water was allowed to stand until heated to room temperature so that bubbles caused by the presence of dissolved air in the water could be removed. The test bath was fitted with a valved drain, flush with the tank bottom, so that the salt water could be removed from time-to-time.

The jet injectors were smooth round glass tubes having inside diameters of 3.2, 6.4 and 12.7 mm. Injector passage length/diameter ratios were 50 to help ensure turbulent flow at the jet exit for sufficiently large jet Reynolds numbers (Wu et al. 1995). The injectors were mounted vertically and discharged roughly 5mm below the liquid surface. The injectors passed through a horizontal plexiglass plate (280 x 432 mm plan dimensions x 12 mm thick) with a tight fit. The injector exits were mounted flush with the lower surface of the plate in order to provide well-defined entrainment conditions near the jet exit. The source liquid was supplied to the injector using up to two syringe pumps (Harvard Apparatus, PHD 2000, Model 70-2000 Syringe Pump, each with four 150 cc syringes mounted in parallel). These pumps were computer controlled to start, stop and deliver liquid at pre-selected times and rates. Pump flow rates were calibrated

by collecting liquid for timed intervals. In addition, start and stop times were monitored using the video records.

The salt water source liquids were prepared by adding appropriate weights of salt (certified ACS crystal sodium chloride, 100.2% assay) to given volumes (weights) of water. Subsequent measurements of the final liquid volumes provided a check of tabulated liquid densities (Lange, 1952). Green and red dyes were added to the source liquid in order to facilitate flow visualization.

**Instrumentation.** Measurements of source flow dimensions as a function of time were obtained from video records. The bath was illuminated for these observations using two 650 W quartz lamps (Color Tran, quartz king dual 650, Model 116-011). The appearance of the dye-containing injected source liquid was recorded as a function of time using a color video CCD camera (Panasonic Model No. WV-CL 352). This camera has a 682 x 492 pixel array (yielding a resolution of 0.5 mm per pixel) with an 8-bit dynamic range, and a 12 mm focal length x f 1.8 lens (WV aspherical-LA/208). Color still photographs of the flows were also obtained with a Nikon FM2 camera having an 85 mm focal length x f 1.4 lens and using conventional Fuji-color film.

The video records were analyzed to provide the maximum mean streamwise penetration distance (taken as the average of the largest streamwise distance of injected source liquid from the jet exit) and the mean maximum radial penetration distance as a function of time from the start of injection. These mean values were obtained by averaging the results of ten separate tests at a particular jet exit condition. Experimental uncertainties (95% confidence) of the various measurements of the video records were as follows: times from the start of injection within 7%, mean maximum streamwise penetration distances within 8% and mean maximum radial penetration distances within 15%. The experimental uncertainty of the time measurements was largely governed by the discretization errors of the video records. The experimental uncertainties of the streamwise and radial penetration distances, however, were largely governed by sampling errors of the irregular boundaries of the present turbulent source liquid flows.

**Test Conditions.** The test conditions for the present round turbulent nonbuoyant starting jets and puffs and buoyant starting plumes and thermals are summarized in Table 1. The test conditions involve jet exit diameters of 3.2-12.7 mm, jet exit Reynolds numbers of 1450-11700 and jet/ambient density ratios of 1.00-1.12. In addition, various amounts of injected liquids were considered for the puffs and thermals, comprising liquid columns having the same diameter as the jet exit and lengths in the range 2-80 source diameters. Finally, the buoyant flows had initial Froude numbers of 1-20, providing

values both larger and smaller (or both under-and over-accelerated initial flows) than the asymptotic value of roughly 5 for stationary self-preserving round buoyant turbulent plumes (George et al., 1977).

**Table 1 Summary of test conditions and scaling properties<sup>a</sup>**

Property	Jet	Puff	Plume	Thermal
$\rho_o(\text{kg/m}^3)$	998	998	1060-1120	1060-1120
$v_o(\text{mm}^2/\text{s})$	1	1	1-2	1-2
$Q_o/(A_o d)$	---	2-80	---	2-80
$Fr_o (-)$	---	---	1-20	1-20
$x_o/d (-)$				
$n (-)$	1/2	1/4	3/4	1/2
$C_x (-)$	2.6	1.9	2.2	2.7
$C_r (-)$	0.16	0.23	0.18	0.22

<sup>a</sup>Salt water solutions injected vertically downward from a round tube into still fresh water with an ambient pressure and temperature of  $99.0 \pm 0.5$  kPa and  $297 \pm 0.5$  K. and source passage length/diameter ratio of 50:1. Other test properties are as follows:  $d = 3.2\text{-}12.7$  mm,  $\dot{Q} = 7\text{-}30$  cc/s,  $Re_o = 1,450\text{-}11,700$ ,  $\rho_\infty = 998$  kg/m<sup>3</sup> and  $v_\infty = 1.0$  mm<sup>2</sup>/s.

### 3. Theoretical Methods

**Preserving Region.** Two parameters that are useful for estimating when turbulent flows from steady and interrupted sources become self-preserving are the distance from the virtual origin normalized by the source diameter,  $(x-x_o)/d$ , and distance from the virtual origin normalized by the Morton length scale,  $(x-x_o)/l_M$  (Dai et al., 1994). The first parameter is pertinent to both nonbuoyant and buoyant flows and measures the

distance needed to modify distributions of mean and fluctuating properties from conditions within a passage to conditions in an unbounded flow (e.g., to eliminate source disturbances). The second parameter is only pertinent to buoyant flows and measures the distance required for buoyancy-induced momentum to become large compared to the source momentum so that the buoyant features of the flow are dominant. The Morton length scale is defined as follows for round buoyant sources having uniform properties (Morton, 1959; List, 1982):

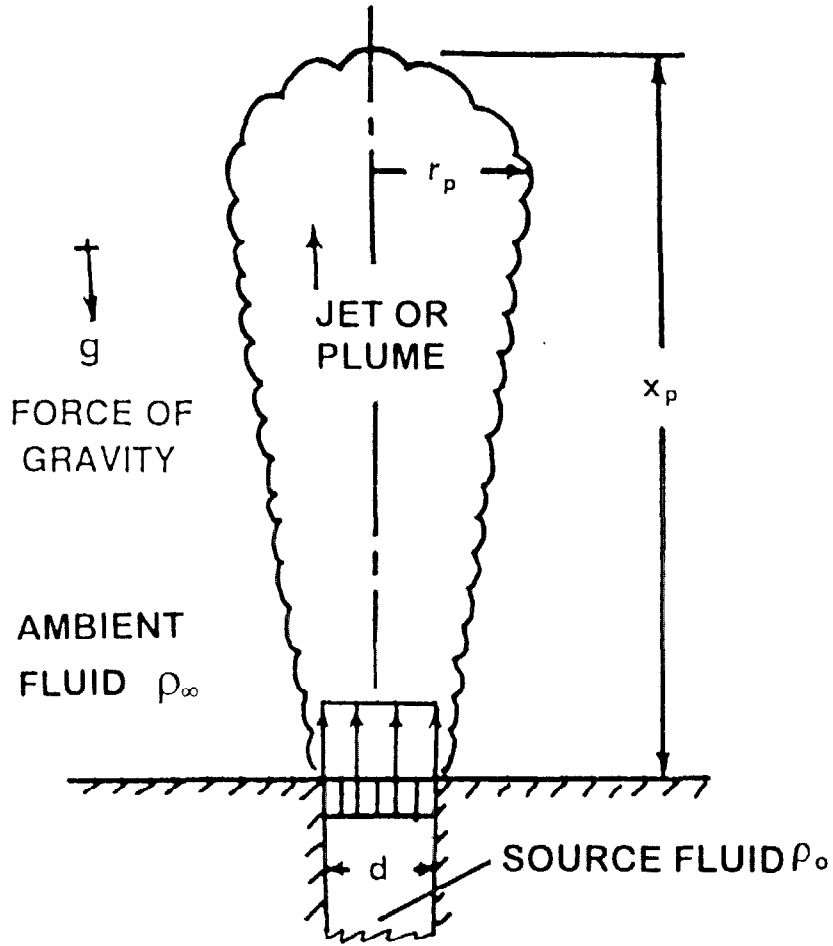
$$l_M/d = (\pi/4)^{1/4} (\rho_\infty u_o^2 / (gd |\rho_o - \rho_\infty|))^{1/2} \quad (1)$$

where an absolute value has been used for the density difference to account for both rising and falling flows. The source Froude number,  $Fr_o$ , is proportional to  $l_M/d$  for uniform source properties, as follows (Dai et al., 1994):

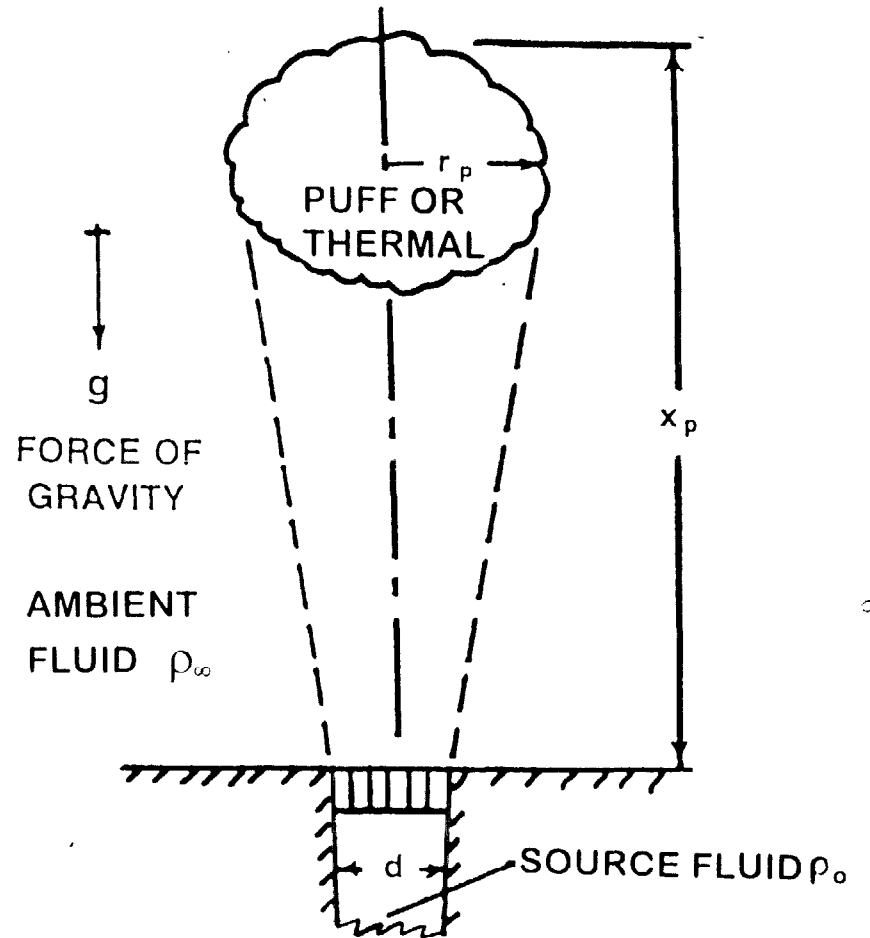
$$Fr_o = (4/\pi)^{1/4} l_M/d \quad (2)$$

and is often used to characterize the initial degree of buoyant behavior of the source, e.g.,  $Fr_o = 0$  and  $\infty$  for purely buoyant and purely nonbuoyant sources, respectively. Past work with steady round turbulent buoyant plumes suggests  $(x-x_o)/d > 80$  and  $(x-x_o)/l_M > 10$  for self-preserving conditions, see Dai et al. (1994) and references cited therein. Another important criterion for self-preserving flows is that properties within the flow should not be very different from ambient properties so that property changes are nearly linear functions of the degree of mixing. For present flows, where the main property variation involves the density, this last criterion for self-preserving behavior implies  $|\rho_{\max} - \rho_\infty|/\rho_\infty \ll 1$ .

**Self-Preserving Scaling.** Assuming that the flow is within the self-preserving region, expressions for the streamwise penetration distance of the present round turbulent flows from steady and interrupted sources are either available from past work or are readily found using past methods, see Baines et al. (1990), Batt et al. (1984), Delichatsios (1979), Johari and Paduano (1987), Kato et al. (1987), Kouros et al. (1993), Kovaszny et al. (1974), List (1982), Morton (1959), Morton et al. (1956), Pantzloff and Lueptow (1977), Richards (1965), Scorer (1957), Turner (1962, 1964, 1969, 1973) and references cited therein. The configurations of the present buoyant and nonbuoyant flows for these analyses are similar as sketched in Fig 1; the main difference between these flows is that  $g = 0$  for the nonbuoyant flows. Both steady and interrupted sources are illustrated in Fig. 1, with the latter leading to puffs and thermals for nonbuoyant and buoyant flows, respectively.



**STEADY SOURCE**



**INTERRUPTED SOURCE**

Fig. 1 Sketch of round turbulent flows from steady and interrupted sources.

Major assumptions for present considerations are similar to earlier analyses to find self-preserving flow scaling: physical property variations in the flows are assumed to be small, steady sources start instantly and subsequently maintain constant source properties, interrupted sources start and stop instantly and maintain constant source properties during the period of flow, and virtual origins are used to maximize conditions where self-preserving behavior is observed. Finally, for convenience, source properties are assumed to be uniform similar to the conditions required for Eqs. (1) and (2). This last approximation is not a critical assumption, however, because the details of the sources are not important, whereas conserved properties of the flows are adequately prescribed by mean source properties, within the self-preserving regions of the present flows.

Under these assumptions, the temporal variation of the maximum streamwise penetration distance can be expressed as follows within the self-preserving regions of the present unsteady turbulent flows:

$$(x_p - x_0)/d = C_x(t/t^*)^n \quad (3)$$

The corresponding temporal variation of the maximum radial penetration distance can be expressed most conveniently in terms of the streamwise penetration distance, as follows:

$$r_p/(x_p - x_0) = C_r \quad (4)$$

The values of  $C_x$ ,  $C_r$ ,  $t^*$  and  $n$  vary depending upon the particular starting flow that is being considered. The values of  $C_x$  and  $C_r$  are best fit empirical parameters of the self-preserving analyses and will be considered later when the measurements are discussed. The values of  $t^*$  and  $n$ , however, follow from the requirements for self-preserving flows and can be expressed as follows for the present unsteady flows:

$$t^* = d/u_0, \quad n = 1/2; \text{ nonbuoyant starting jet} \quad (5)$$

$$t^* = d/u_0, \quad n = 1/4; \text{ nonbuoyant puff} \quad (6)$$

$$t^* = (d^4/\dot{B}_0)^{1/3}, \quad n = 3/4; \text{ buoyant starting plume} \quad (7)$$

$$t^* = (d^4/B_0)^{1/2}, \quad n = 1/2; \text{ buoyant thermal} \quad (8)$$

where  $\dot{B}_0$  is a buoyant flux for a plume and  $B_0$  is a buoyant force for a thermal, e.g.,

$$\dot{B}_0 = \dot{Q}_0 g |\rho_0 - \rho_\infty| / \rho_\infty; \quad \text{buoyant starting plume} \quad (9)$$

$$B_o = Q_o g |\rho_o - \rho_\infty| / \rho_\infty; \quad \text{buoyant thermal} \quad (10)$$

and an absolute value has been used for the density difference, as before, to account for both rising and falling flows.

#### 4. Results and Discussion

**Approach.** Results for nonbuoyant starting jets, nonbuoyant puffs, buoyant starting plumes and buoyant thermals are discussed in turn in the following. Findings for each flow include visualization of the flow, correlation of measured streamwise penetration distances as a function of time with the appropriate self-preserving scaling law from Eqs. (3), and correlation of measured maximum radial penetration distances as a function of time with the appropriate self-preserving scaling law from Eqs. (4). The ranges of test conditions and the best fit values of  $x_o/d$ ,  $n$ ,  $C_x$  and  $C_r$  for the scaling laws based on the present measurements of the various flows are summarized in Table 1.

**Starting Nonbuoyant Jets.** Video images of a typical round nonbuoyant starting turbulent jet at various times after initiation of the flow are illustrated in Fig. 2. At this test condition, the flow boundary is relatively smooth near the jet exit but becomes roughened and turbulent-like a few diameters from the jet exit at small times after the start of injection. With increasing time, however the transition to a roughened surface shifts toward the jet exit, a trend that has been observed by others for starting flows, see Kato et al. (1987). The turbulent region of the flow extends from the transition condition to the farthest streamwise penetration location of the nonbuoyant starting jet, which includes the vortex at the tip of the flow. The flow radius is seen to vary smoothly from the jet exit to the maximum radius condition near the tip of the flow with no tendency to form a cap-like structure associated with the leading vortex (the image at 4530 ms is somewhat untypical in this respect). This behavior of the flow radius is also similar to other observations of starting jets (Kato et al., 1987).

Normalized streamwise penetration distances of starting jets are plotted according to the self-preserving scaling of Eqs. (3) and (5) in Fig. 3. Near-source penetration properties exhibit a variety of behaviors depending on source properties, however, all the measurements follow the self-preserving correlation reasonably well at large dimensionless times, e.g.,  $t_u/d > 100$ . These conditions correspond to normalized streamwise penetration distances,  $(x_p - x_o)/d > 30$ , which is much nearer to the source than values of  $(x - x_o)/d > 100$  needed to reach self-preserving behavior for steady round buoyant turbulent plumes based on measured mean concentrations and velocity

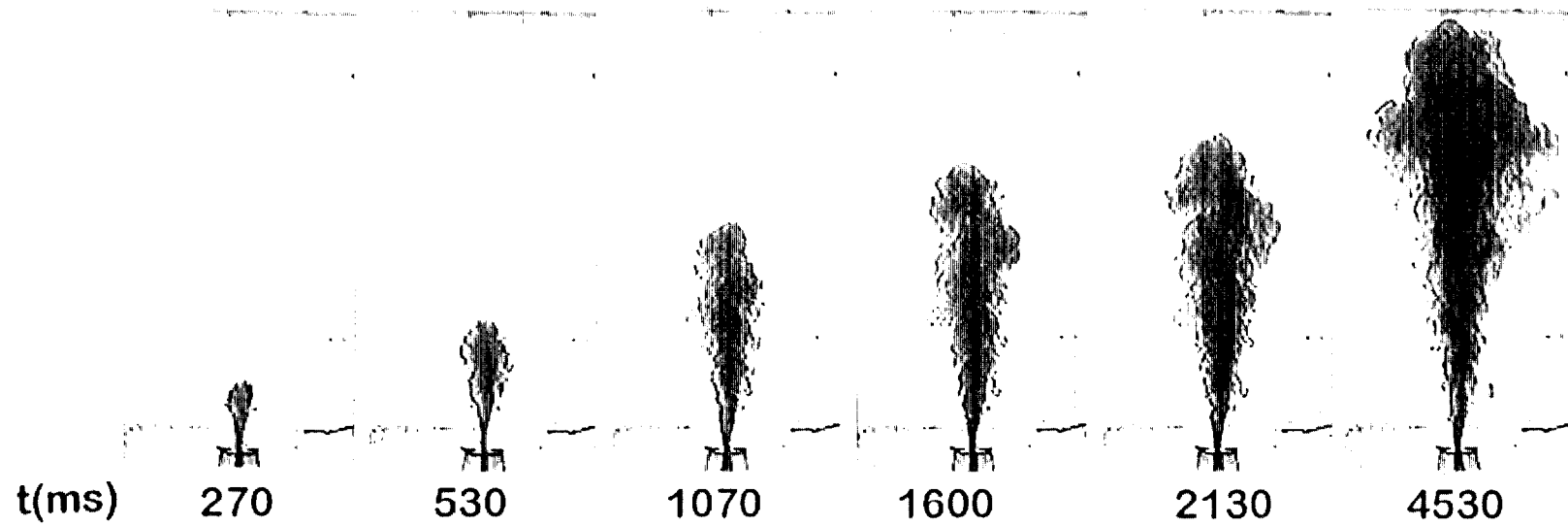


Fig. 2 Visualization of a round turbulent nonbuoyant starting jet ( $d=6.4$  mm,  $u_0 = 46$  mm/s,  $Re_0 = 2950$ ).

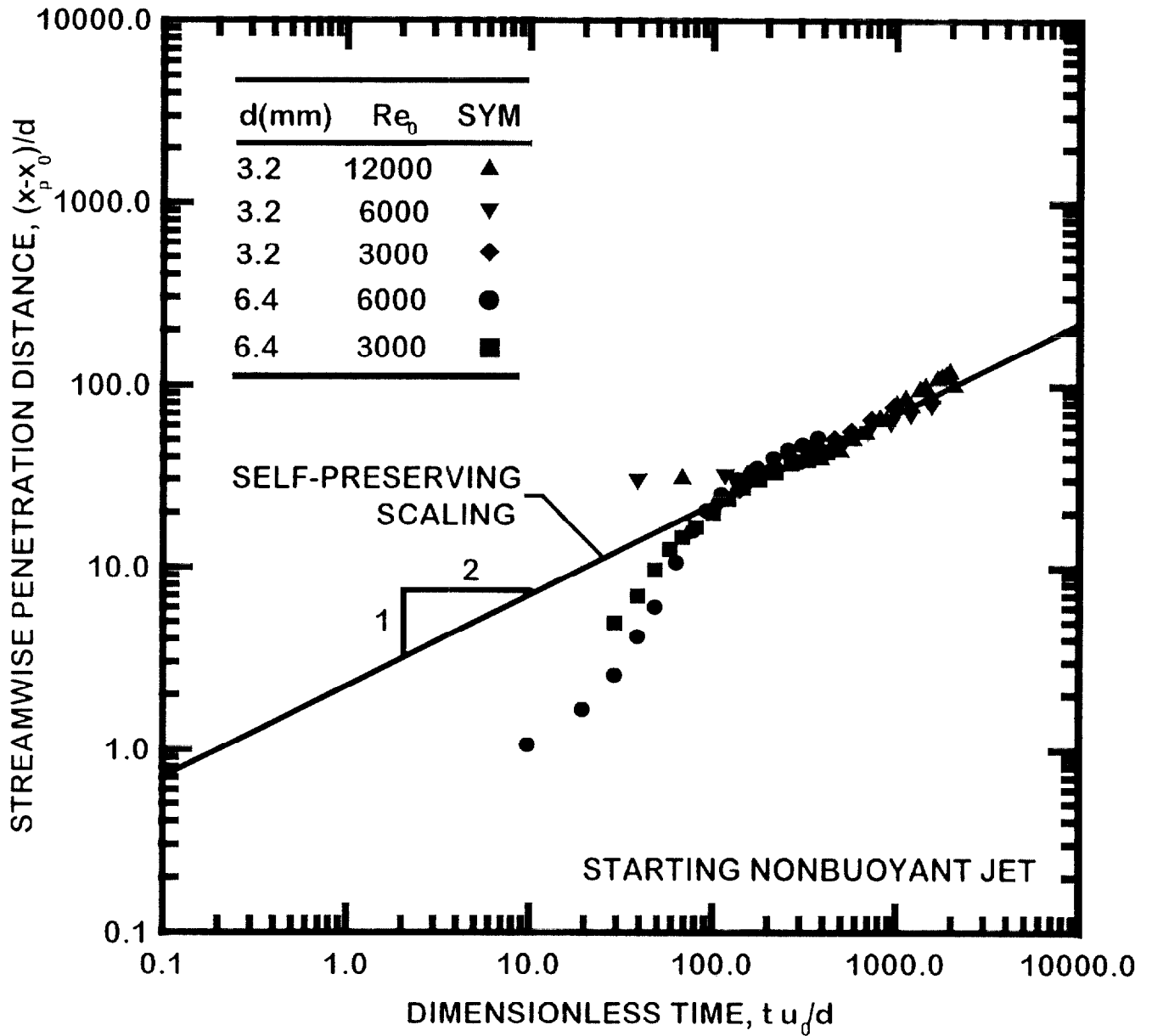


Fig. 3 Penetration distance as a function of time for round turbulent nonbuoyant steady jets.

distributions (Dai et al., 1994, 1995). A possible explanation for these differences could be the different fundamental stabilities of starting and steady turbulent flows; another factor is that self-preserving behavior frequently is established at different distances from the source depending on the property that is observed (Dai et al., 1994,1995).

Normalized maximum radial penetration distances of starting jets are plotted according to the self-preserving scaling of Eq. (4) in Fig. 4. The normalized radial penetration distance has relatively large values in the region nearest the source where measurements were made; such behavior is expected, however, because this property becomes infinitely large at the virtual origin. The normalized maximum radial penetration distance decreases at first with increasing streamwise distance and after reaching a minimum at  $(x_p-x_0)/d$  of 15-30, becomes relatively constant in the self-preserving region where  $(x_p-x_0)/d > 30$ . For self-preserving conditions,  $r_p/(x_p-x_0) = C_r = 0.16$  from Table 1 which is shown on the plot for references purposes. This value is comparable to the outer boundary of steady round turbulent jets based on measured distributions of mean velocities and mixture fractions, see Hinze (1975). It is also evident from the jet images of Fig. 2 that this value of  $r_p/(x-x_0)$  is maintained along the sides of the jet within the self-preserving region.

**Nonbuoyant Puffs.** Video images of a typical round nonbuoyant turbulent puffs at various times after initiation of the flow are illustrated in Fig. 5. The present observations of both puffs and thermals are qualitatively similar to earlier observations of thermals in the literature due to Scorer (1957) and Turner (1962). The appearance of flow in the early stages when the source flow is maintained is naturally identical to the starting jet. When the source flow is terminated, however, the leading turbulent vortex and the starting jet continue to penetrate into the still liquid with a thin stem connecting the base of the interrupted jet to the source. The stem continues to be stretched as the vortex and starting jet move away from the jet exit but the fluid velocity within the stem appears to be small and only a small fraction of the injected fluid was associated with the stem for most of the test conditions considered during the present investigation. The main difference between the motion of the upper regions of a starting jet and a puff is that the latter has a much smaller velocity once the source flow has been interrupted, which is evident from the different scaling of starting jets and puffs from Eqs. (3), (5) and (6), e.g.,  $x_p \sim t^n$  with  $n = 1/2$  and  $1/4$  respectively for starting jets and puffs. Another interesting contrast between starting jets and puffs is that the properties of the latter are affected by the amount of source fluid used to form the puff. Large amounts of source fluid, as in Fig. 5, yield a leading vortex followed by an extended jet-like region. Reduced amounts of source fluid, and continued penetration into the ambient fluid, reduce the extent of the wake-like region and eventually the leading vortex as well, see Scorer (1957).

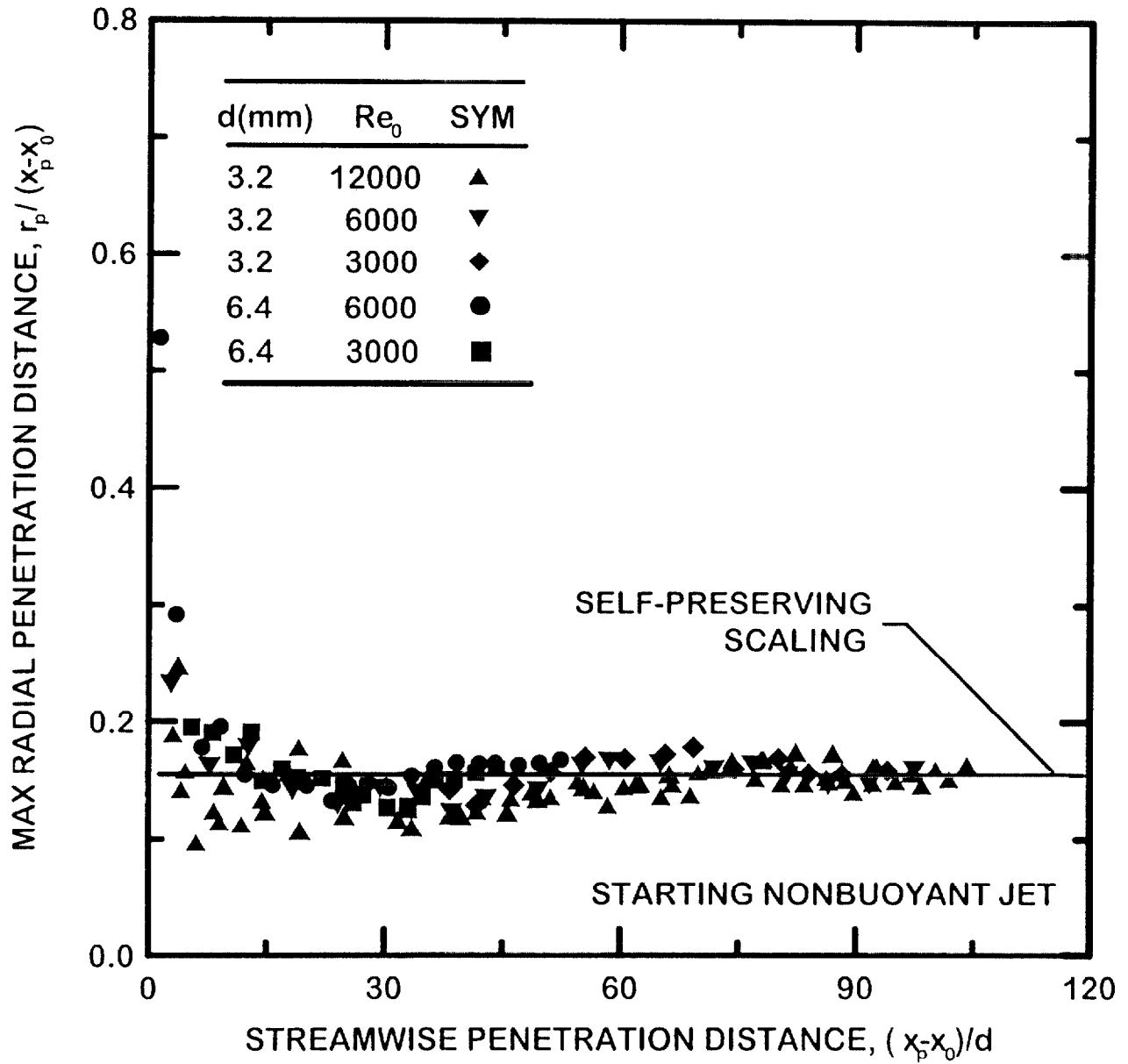


Fig. 4 Flow radius as a function of penetration distant for round turbulent nonbuoyant steady jets.

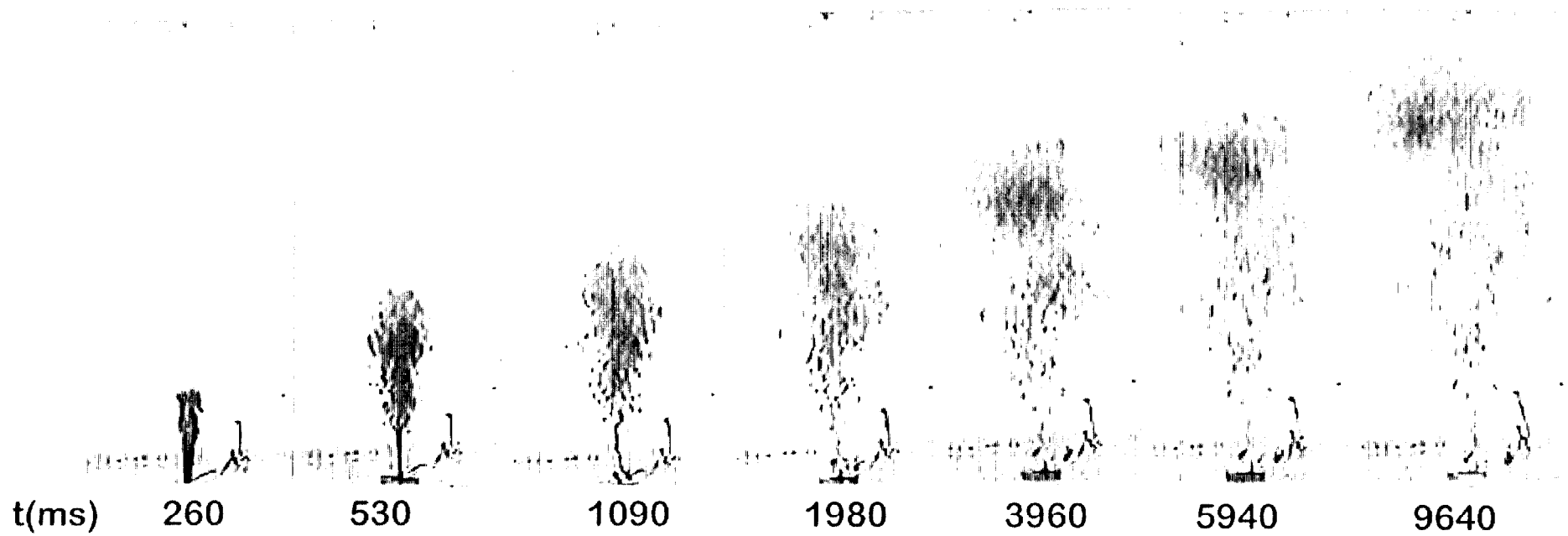


Fig. 5 Visualization of a round turbulent nonbuoyant puff ( $d=6.4$  mm,  $u_o = 93$  mm/s,  $Re_o = 5900$ ,  $Q_o/(A_o d) = 50$ ).

Normalized streamwise penetration distances of puffs are plotted according to the self-preserving scaling of Eqs. (3) and (6) in Fig. 6. Present measurements agree reasonably well with self-preserving scaling for  $tu_0/d > 100$ , and  $(x_p-x_0)/d > 30$ , similar to the starting jet. The different powers of the temporal growth of puffs compared to the starting jets,  $n = 1/4$  compared to  $1/2$ , results in a much slower streamwise growth rate for puffs because the momentum supplied by the source is interrupted.

Normalized maximum radial penetration distances for puffs are plotted according to the self-preserving scaling of Eq. (4) in Fig. 7. The behavior here is qualitatively similar to results for the starting jet illustrated in Fig. 4; the main difference is that the normalized maximum radial penetration distance in the self-preserving region is larger for puffs than starting jets, e.g.,  $r_p/(x_p-x_0) = C_r = 0.23$  compared to 0.16, see Table 1. This radial penetration distance for puffs is comparable to results for buoyant thermals from the present study and from Scorer (1957), where  $r_p/(x_p-x_0) = 0.22$  and 0.25, respectively.

**Starting Buoyant Plumes.** Video images of a typical starting round buoyant turbulent plume at various times after the initiation of the flow are illustrated in Fig. 8. The general appearance of starting nonbuoyant jets and starting buoyant plumes is similar, cf., Figs. 2 and 8, even though the scaling of these flows differs. The starting plumes generally exhibited roughened surfaces nearer to the jet exit than starting jets at comparable source conditions which is consistent with the widely recognized increased instability of plumes compared to jets. The radius of the plume is also seen to increase smoothly from the jet exit, with no evidence of a cap-like structure associated with the leading vortex.

Normalized streamwise penetration distances for starting plumes are plotted according to the self-preserving scaling of Eqs. (3) and (6) in Fig. 9. Present measurements agree reasonably well with self-preserving scaling for  $t\dot{B}_0^{1/3}/d^{4/3} > 20$  and  $(x_p-x_0)/d > 20$ , suggesting a somewhat faster rate of development of starting buoyant plumes than nonbuoyant jets toward self-preserving behavior. The rate of growth of the plumes is also faster for starting plumes than for the other flows at comparable source conditions due to enhanced motion caused by effects of buoyancy as well as continued source inflow, e.g.,  $n=3/4$  for starting plumes which is larger than the rest, see Table 1.

Normalized maximum radial penetration distances for starting plumes are plotted according to the self-preserving scaling of Eq. (4) in Fig. 10. These results are also similar to the other starting flows with  $r_p/(x_p-x_0) = C_r = 0.18$  in the self-preserving region.

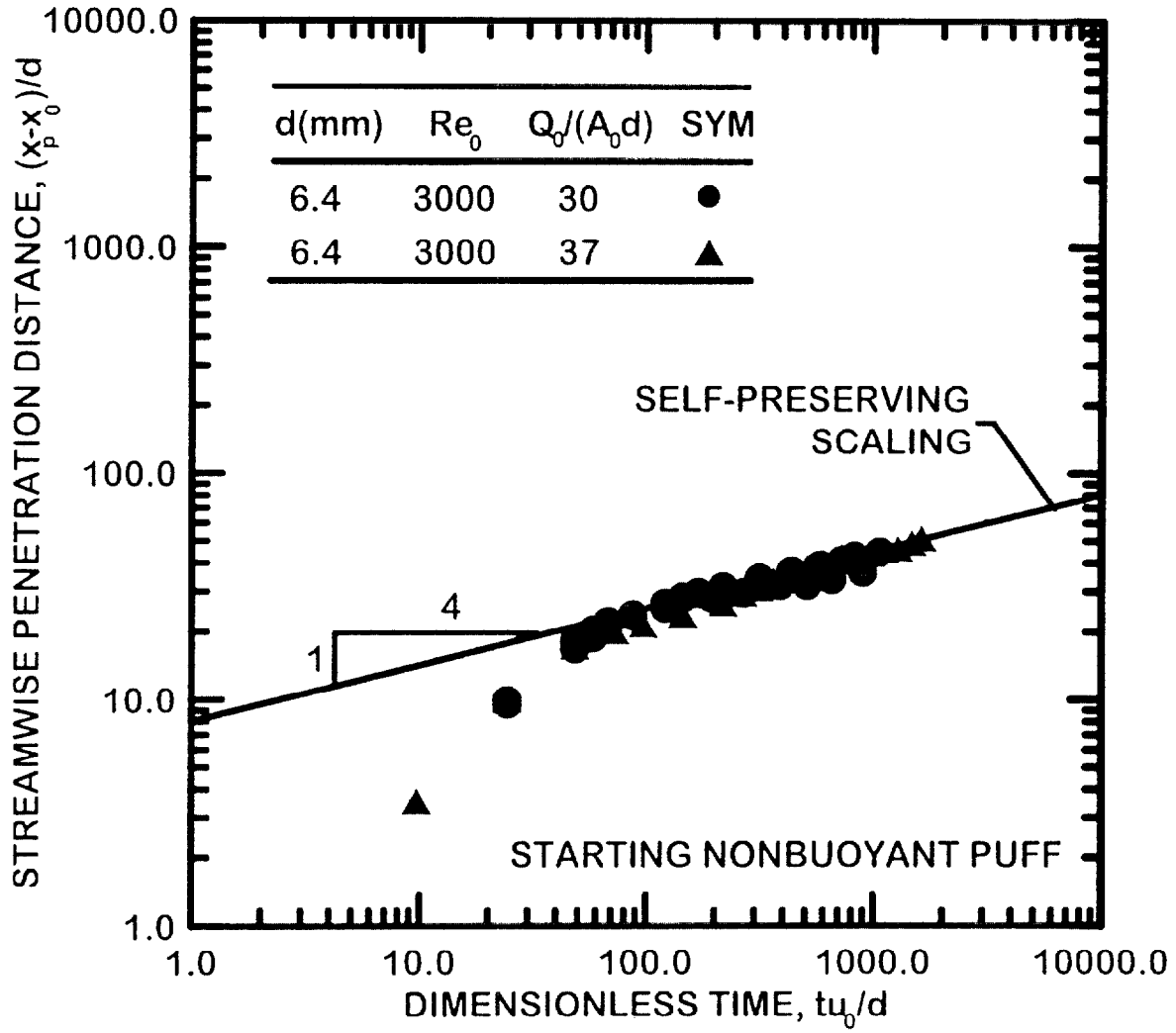


Fig. 6 Penetration distance as a function of time for round turbulent nonbuoyant puffs.

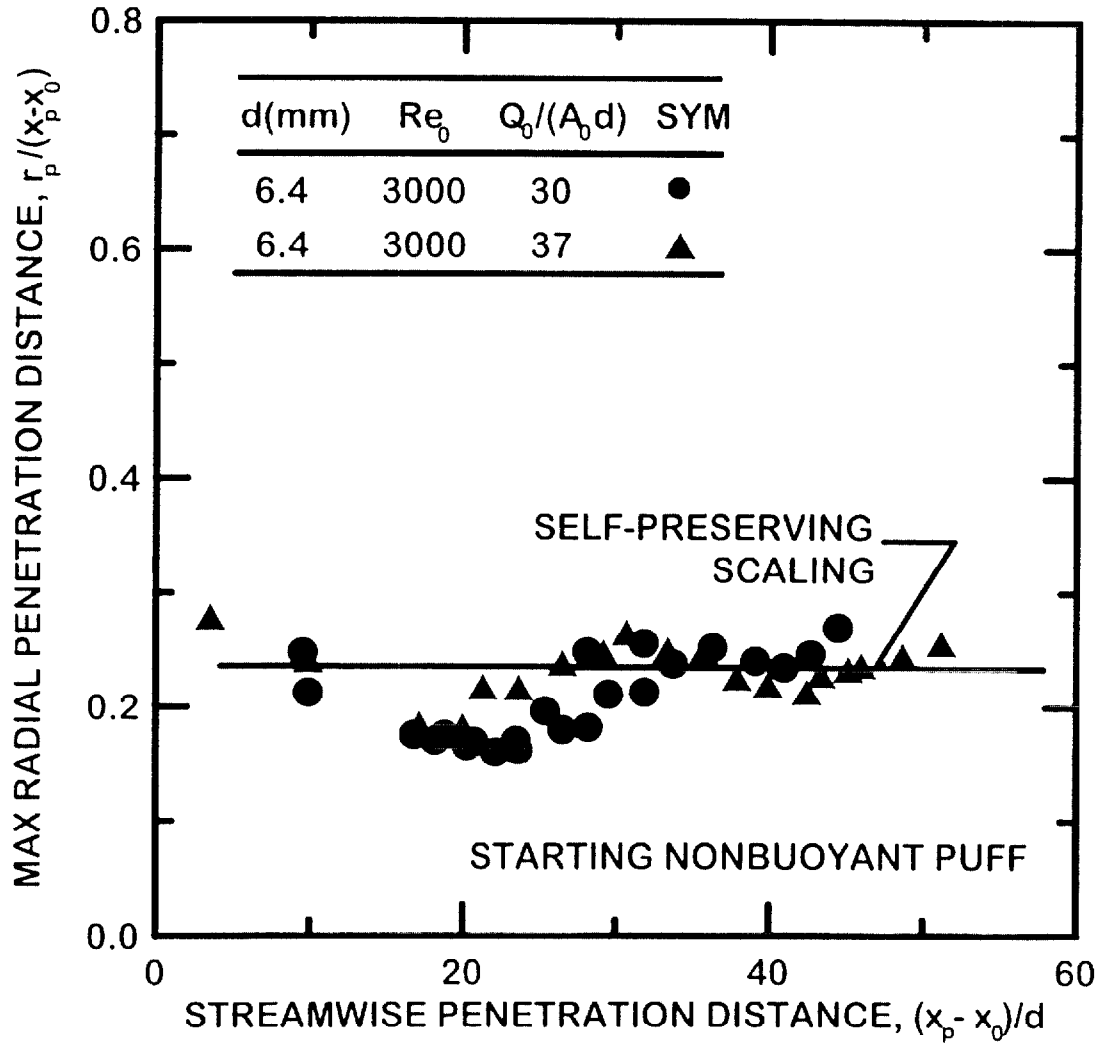


Fig. 7 Flow radius as a function of penetration distance for round turbulent nonbuoyant puffs.

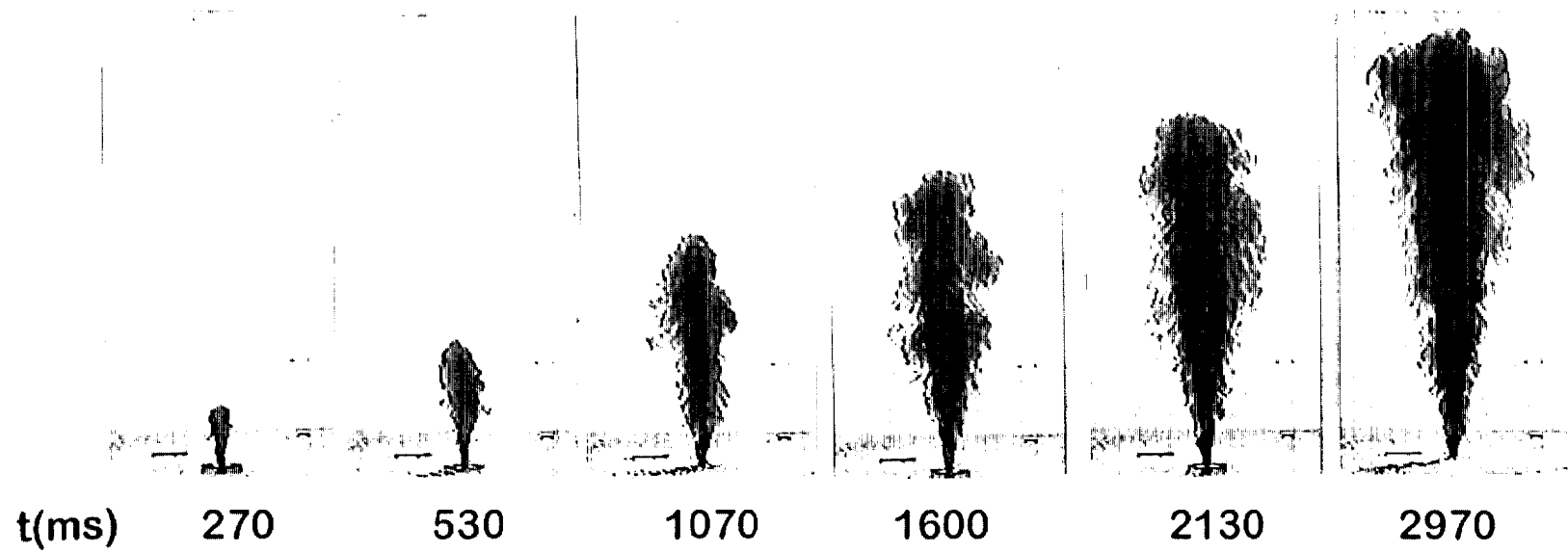


Fig. 8 Visualization of a round turbulent starting buoyant plume ( $d = 6.4$  mm,  $u_o = 46$  mm/s,  $Re_o = 3200$ ,  $\rho_o/\rho_\infty = 1.076$ ,  $Fr_o = 7.0$ ).

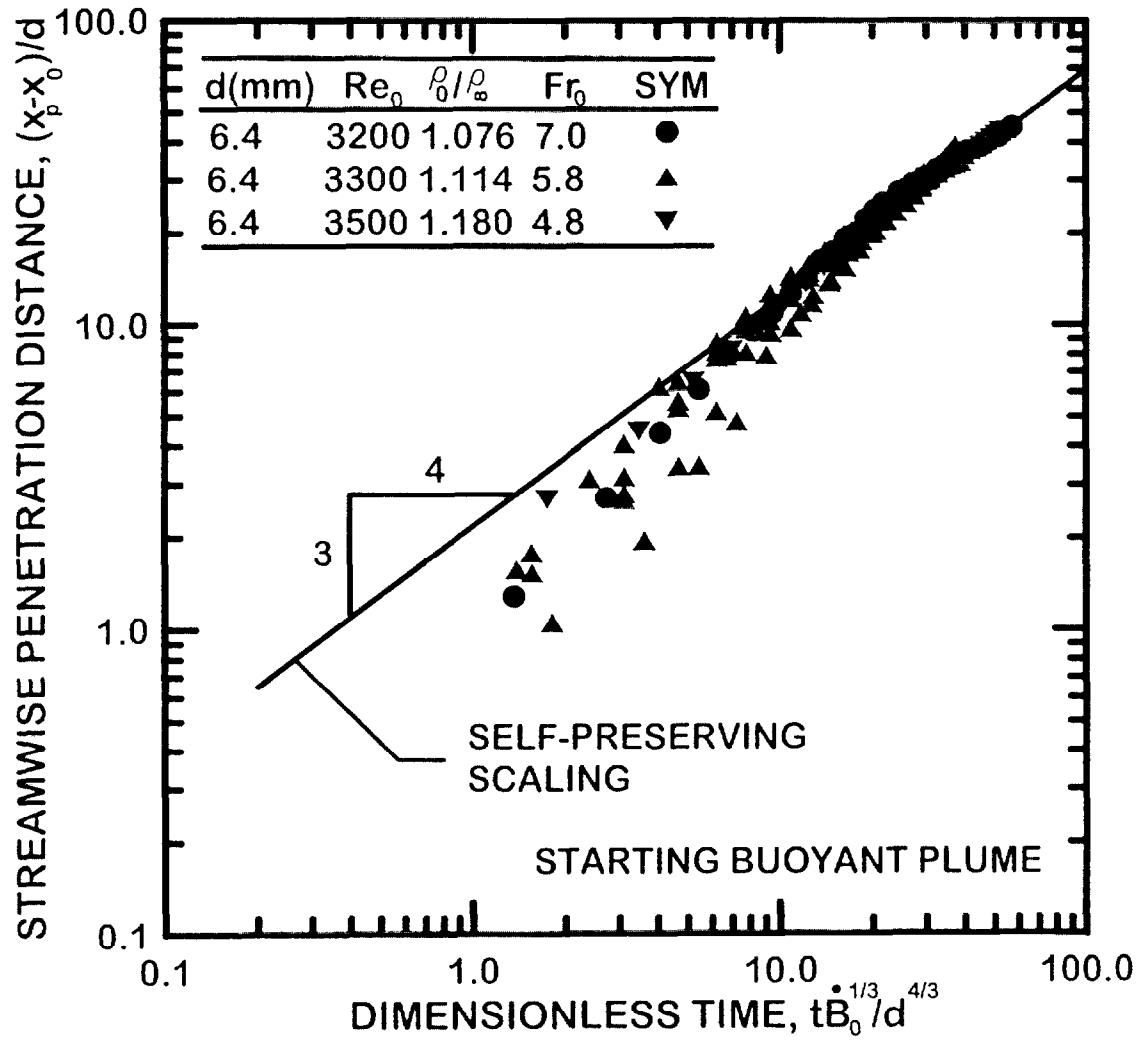


Fig. 9 Penetration distance as a function of time for round turbulent buoyant steady plumes.

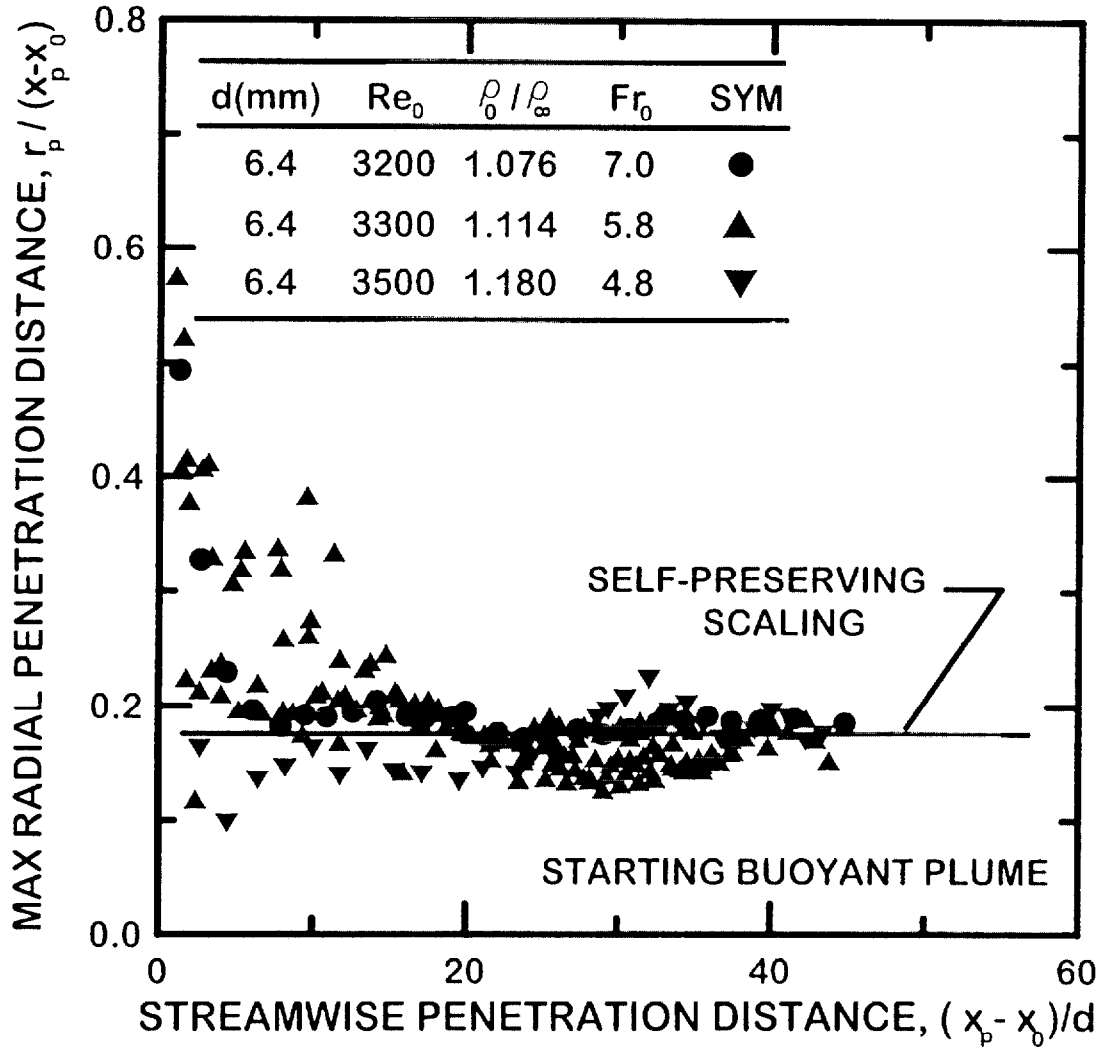


Fig. 10 Flow radius as a function of penetration distance for round turbulent buoyant plumes.

This value is comparable to results observed for steady buoyant turbulent plumes (Dai, 1994, 1995) and both starting and steady jets (Hinze, 1975).

**Buoyant Thermals.** Video images of a typical round buoyant turbulent thermal at various times after the initiation of the flow are illustrated in Fig. 11. Some interesting differences can be seen between the appearance of puffs and thermals, Figs. 8 and 11. In particular, the buoyancy induced motion in a thermal causes the stem between the plume-like region of the flow and the source to disappear relatively rapidly for thermals compared to puffs. The buoyant motion also causes the plume-like region of the flow in thermals to merge relatively rapidly with the leading vortex compared to puffs. On the other hand, the variation of maximum radial penetration distances with streamwise penetration distances is similar for thermals and puffs, whereas both are larger than the corresponding radial penetration distance for starting jets and plumes.

Normalized streamwise penetration distances for thermals are plotted according to the self-preserving scaling of Eqs. (3) and (7) in Fig. 12. Present measurements agree reasonably well with self-preserving scaling for  $t B_o^{1/2}/d^2 > 20$  and  $(x_p - x_o)/d > 20$ , suggesting comparable rates of development of thermals and starting plumes toward self-preserving behavior. The rate of growth of thermals and starting jets is comparable, i.e.,  $n = 1/2$  in both cases, because effects of buoyancy tend to compensate for the interrupted source flow for thermals.

Normalized maximum radial penetration distances for thermals are plotted according to the self-preserving scaling of Eq. (4) in Fig. 13. These results are similar to the other flows with  $r_p/(x_p - x_o) = 0.22$  in the self-preserving region, similar to the value observed for puffs.

## 5. Conclusions

The temporal development of round turbulent nonbuoyant starting jets and puffs and buoyant starting plumes and thermals was studied both theoretically and experimentally. Conditions far from the source were emphasized where effects of source disturbances are lost, where the conserved properties of the flow control flow structure and where self-preserving behavior is approximated. The test conditions consisted of salt or fresh water sources injected vertically downward into still and unstratified fresh water with injector passage length/diameter ratios of 50 and test conditions as follows: jet exit diameters of 3.2-12.7 mm, jet exit Reynolds numbers of 1450-11700, and jet/ambient density ratios of 1.00-1.12. The major conclusions of the study are as follows:

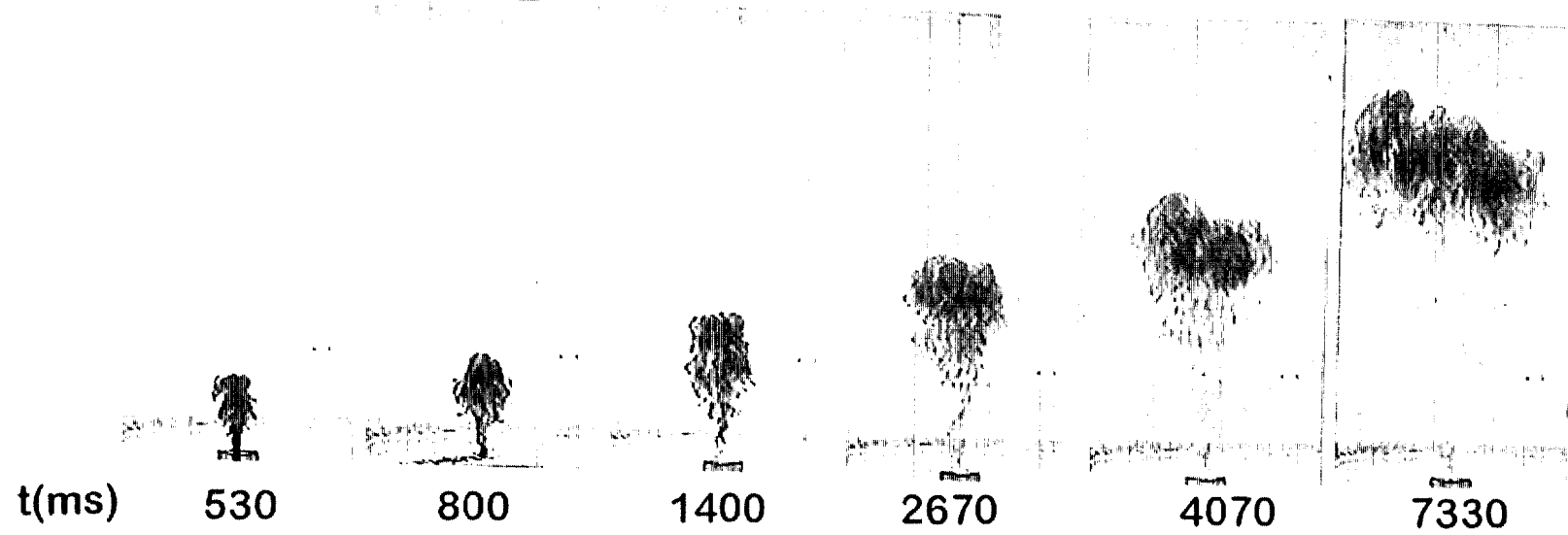


Fig. 11 Visualization of a round turbulent buoyant thermal ( $d = 6.4$  mm,  $u_o = 46$  mm/s,  $Re_o = 3200$ ,  $\rho_o/\rho_\infty = 1.084$ ,  $Fr_o = 6.7$ ,  $Q_o/(A_o d) = 10$ ).

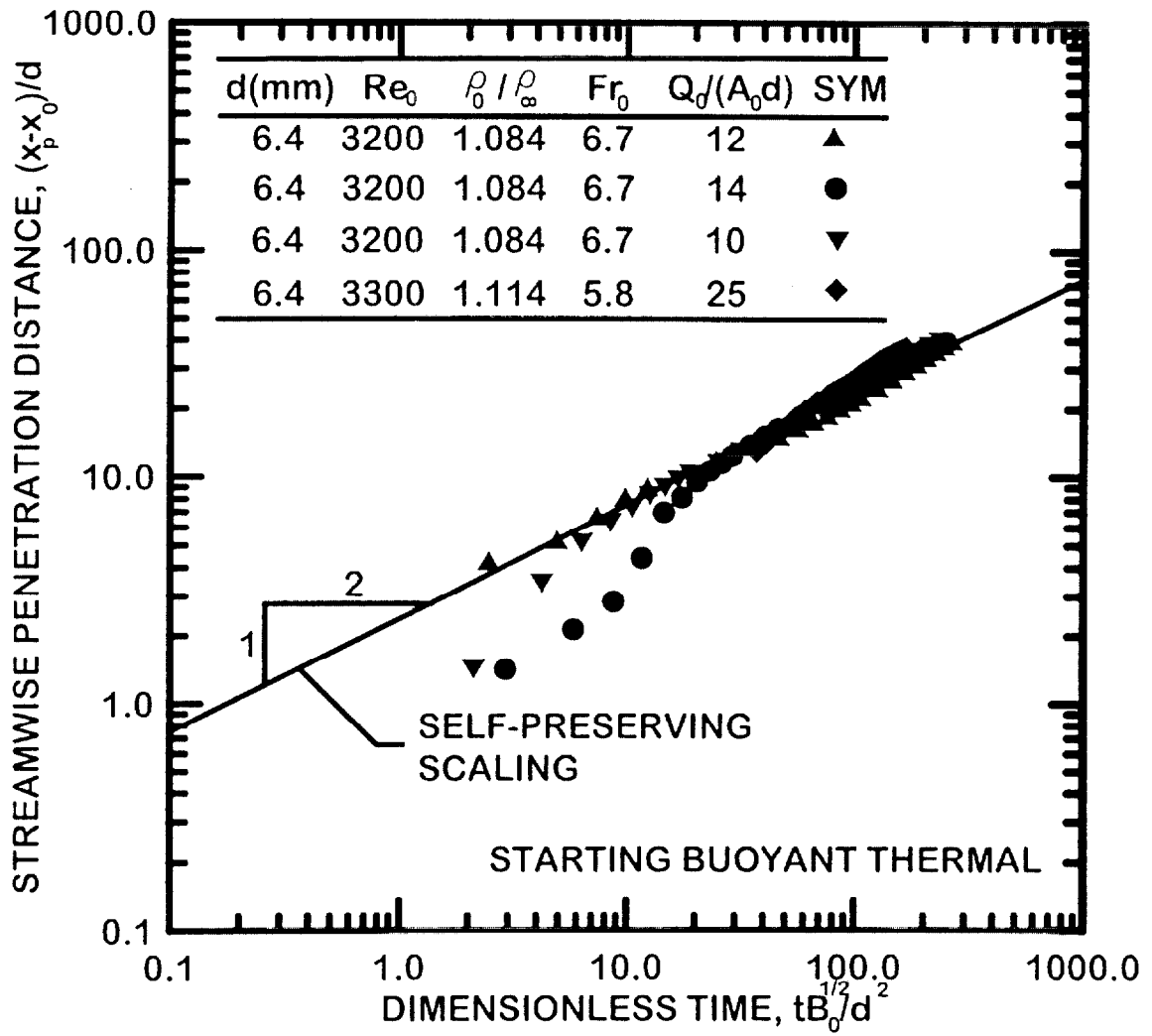


Fig. 12 Penetration distance as a function of time for round turbulent buoyant thermals.

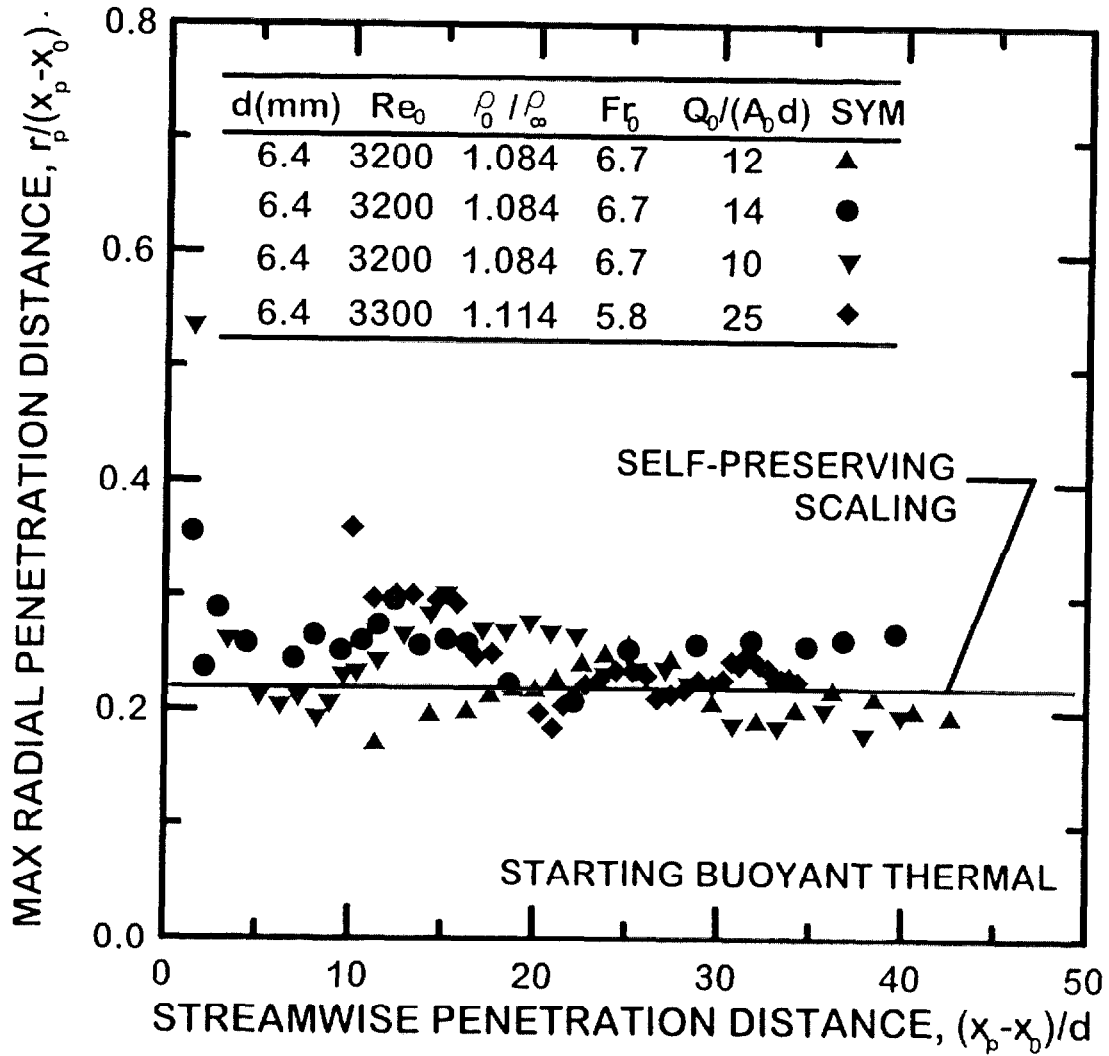


Fig. 13 Flow radius as a function of penetration distance for round turbulent buoyant thermals.

1. The present flows became turbulent near the jet exit, at distances of 0-5 source diameters; and although near-source behavior varied significantly with source properties, self-preserving behavior was generally observed at distances greater than 20-30 source diameters from the source.
2. Within the self-preserving region, the dimensionless penetration distance,  $(x_p - x_0)/d$ , generally varied as a function of time in agreement with self-preserving predictions. This implies that the maximum penetration distance varied as a function of time to the following powers:  $1/2$ (nonbuoyant starting jet),  $1/4$ (nonbuoyant puff),  $3/4$ (buoyant starting plume) and  $1/2$ (buoyant thermal).
3. Within the self-preserving region, the normalized maximum radius of the flow generally grew as a function of time in the same manner as the normalized penetration distance. This implies the following normalized values of maximum flow radius,  $r_p/(x_p - x_0)$ : 0.16(nonbuoyant starting jet), 0.23(nonbuoyant puff), 0.18(buoyant starting plume) and 0.22(starting buoyant thermal). These maximum radii were observed at the position of the leading vortex.

### References

- Baines, W.D., Turner, J.S., and Campbell, I.H. (1990) "Turbulent Fountains in an Open Chamber," J. Fluid Mech., Vol. 212, pp. 557-592.
- Batt, R.G., Brigoni, R.A., and Rowland, D.J. (1984) "Temperature-Field Structure Within Atmospheric Buoyant Thermals," J. Fluid Mech., Vol. 141, pp. 1-25.
- Baum, H.R., McGrattan, K.B., and Rehm, R.G. (1994) "Simulation of Smoke Plumes from Large Pool Fires," *Twenty-Fifth Symposium (International) on Combustion*, The Combustion Institute, Pittsburgh, pp. 1463-1469.
- Dai, Z., Tseng, L.-K., and Faeth, G.M.(1994) "Structure of Round, Fully-Developed, Buoyant Turbulent Plumes," J. Heat Trans., Vol.116, pp. 409-417.
- Dai, Z., Tseng, L.-K, and Faeth, G.M. (1995) "Velocity Statistics of Round, Fully-Developed Buoyant Turbulent Plumes," J. Heat Transfer, Vol. 117, pp. 138-145.
- Delichatsios, M.A. (1979) "Time Similarity Analysis of Unsteady Buoyant Plumes," J. Fluid Mech., Vol. 93, pp. 241-250.

Fay, J.A., and Lewis, D.H. (1976) "Unsteady Burning of Unconfined Fuel Vapor Clouds," *Sixteenth Symposium (International) on Combustion*, The Combustion Institute, Pittsburgh, pp. 1397-1405.

George, W.K., Jr., Alpert, R.L., and Tamanini, F. (1977) "Turbulence Measurements in an Axisymmetric Buoyant Plume," Int. J. Heat Mass Trans., Vol. 20, pp. 1145-1154.

Hinze, J.O. (1975) *Turbulence*, 2<sup>nd</sup> Ed., McGraw-Hill, New York, pp. 534-585.

Johari, J., and Paduano, R. (1987) "Dilution and Mixing in an Unsteady Turbulent Jet," Experiments in Fluids, Vol. 23, pp. 272-280.

Kato, S.M., Groenwagen, B.C., and Breidenthal, R.E. (1987) "On Turbulent Mixing in Nonsteady Jets," AIAA J., Vol. 25, pp. 165-168.

Kouros, H., Medina, R., and Johari, H. (1993) "Spreading Rate of an Unsteady Turbulent Jet," AIAA J., Vol. 31, pp. 1524-1526.

Kovaszny, L.S.G., Fujita, H., and Lee, R.L. (1974) "Unsteady Turbulent Puffs," Adv. Geophys., Vol. 18B, pp. 253-263.

Lange, N.A. (1952) *Handbook of Chemistry*, Handbook Publishers, Sandusky, Ohio, pp. 1160.

List, E.J. (1982) "Turbulent Jets and Plumes," Ann. Rev. Fluid Mech., Vol. 14, pp. 189-212.

Morton, B.R. (1959) "Forced Plumes," J. Fluid Mech., Vol. 5, pp. 151-163.

Morton, B.R. Taylor, G.I., and Turner, J.S. (1956) "Turbulent Gravitational Convection from Maintained and Instantaneous Sources," Proc. Roy. Soc. London, Vol. A234, pp. 1-23.

Pantzlaff, L., and Lueptow, R.M. (1997) "Transient Character of Positively and Negatively Buoyant Turbulent Jets," Proceedings of the Ocean Engineering Division, OED-Vol. 14, ASME, New York, pp. 81-87.

Richards, J.M. (1965) "Puff Motions in Unstratified Surroundings," J. Fluid Mech., Vol. 21, pp. 97-106.

Sangras, R., Dai, Z., and Faeth, G.M. (1998) "Mixing Structure of Plane Self-Preserving Buoyant Turbulent Plumes," J. Heat Transfer., Vol. 120, pp. 1033-1041.

Sangras, R., Dai, Z., and Faeth, G.M. (1999) "Mixture Fraction Statistics of Plane Self-Preserving Buoyant Turbulent Adiabatic Wall Plumes," J. Heat Trans., Vol. 121, pp. 837-843.

Steckler, K.D., Baum, H.R., and Quintiere, J.G. (1986) "Salt Water Modeling of Fire Induced Flows in Multicomponent Enclosures," *Twenty-First Symposium (International) on Combustion*, The Combustion Institute, Pittsburgh, pp. 143-149.

Scorer, R.S. (1957) "Experiments on Convection of Isolated Masses of Buoyant Fluid," J. Fluid Mech., Vol. 2, p. 583-594.

Turner, J.S. (1962) "The Starting Plume in Neutral Surroundings," J. Fluid Mech., Vol. 13, pp. 356-368.

Turner, J.S. (1964) "The Dynamics of Spheroidal Masses of Buoyant Fluid," J. Fluid Mech., Vol. 19, pp. 481-490.

Turner, J.S. (1969) "Buoyant Plumes and Thermals," Ann. Rev. Fluid Mech., Vol. 1, pp. 29-44.

Turner, J.S. (1973) *Buoyancy Effects in Fluids*, Cambridge University Press, Cambridge, London.

Wu, P.-K., Miranda, R.F., and Faeth, G.M. (1995) "Effects of Initial Flow Conditions on Primary Breakup of Nonturbulent and Turbulent Round Liquid Jets," Atm. Sprays., Vol. 5, pp. 175-196.